p-ISSN 2301–4156 | e-ISSN 2460–5719

Superpixel-Based Stripe Noise Removal for Satellite Imageries

Kamirul[1], Khairunnisa[2], Ega Asti Anggari[3], Dicka Ariptian Rahayu[4], Agus Herawan[5], Moedji Soedjarwo[6], Chusnul Tri Judianto[7]

[1,2,3,4,5,6,7] Research Center for Satellite, The National Research and Innovation Agency (BRIN), Bogor 16310 INDONESIA (tel.: 0251-8621667; fax: 0251-8621667; email: [1]kamirul@brin.go.id, [2]khai010@brin.go.id, [3]egaa001@brin.go.id, [4]dick010@brin.go.id, [5]agus112@brin.go.id, [6]chus002@brin.go.id, [7]moed001@brin.go.id)

[Received: 30 March 2023, Revised: 24 May 2023]
Corresponding Author: Kamirul

ABSTRACT — This work introduces a novel noise removal algorithm for satellite imageries based on superpixel segmentation followed by statistics-based filtering. The algorithm worked in three main steps. First, the noisy input image was divided into subregions by employing simple linear iterative clustering (SLIC)-based superpixel segmentation. Then, the statistical property of each subregion was calculated, including their standard deviations and maximum values. Last, an adaptive statistics-based stripe noise removal was performed for each subregion by constructing adaptive filter sizes according to calculated properties. The algorithm was tested using real satellite imageries taken by the LAPAN-A2 and LAPAN-A3 satellites. Its performance was then compared to three existing methods in terms of image quality and computation speed. Extensive experiments on two datasets of 3-channel images captured by the LAPAN-A2 satellite showed that the algorithm was capable of reducing the stripe pattern as measured using the peak-signal-to-noise-ratio (PSNR) metric without introducing additional artifacts, which commonly appeared on over-corrected regions. Moreover, compared to existing methods, the proposed algorithm ran 42 to 103 times faster and provided better image quality by 2.46%, measured using the structural similarity metric (SSIM). The code of this work and the datasets used for the testing are publicly available on www.github.com/dancingpixel/SPSNR.

KEYWORDS — Stripe, Noise, Imagery, Satellite, LAPAN-A2, LAPAN-A3.

I. INTRODUCTION

Satellite imagery is becoming increasingly popular due to its versatile applications in various fields, such as agriculture, geology, and weather forecasting. As this technology continues to evolve, there is a growing demand for using satellite imagery for mapping, measurement, change detection, and monitoring purposes. This trend is fueled by advancements in satellite technology [1], [2].

As satellite imagery becomes more prevalent in various applications, it is crucial to provide high-quality images free from noise to ensure that the resulting analysis yields useful information that aligns with the desired outcomes. However, providing fine-quality images is challenging due to various factors that may cause the satellite imaging system to produce subpar image quality. These factors can generally be classified into two categories: internal and external factors. Examples of internal factors include the presence of vibration on the satellite while capturing images, misalignment of the on-orbit camera, unstable satellite power, and near expiration of the camera's usage duration. On the other hand, external factors are mainly caused by unfavorable space conditions, such as over-radiation from the sun exposing the satellite system and radio frequency interference (RFI) experienced by the satellite communication link during data transmission [3], [4].

As previously mentioned, internal and external factors can result in subpar image quality in satellite imaging systems, leading to noise in captured images. Additionally, differences in detector response and calibration errors may also contribute to the appearance of noise in images taken by imaging systems such as push-broom and cross-track devices [5]–[7]. These types of noise can obscure the original image and compromise its suitability for subsequent processing, such as image unmixing and classification [8], [9]. Therefore, it is crucial to perform a noise-removal process to enhance the visual quality of images captured by the satellite's imaging system. By providing a noise-free image, subsequent image processing and analysis can be performed accurately.

Various denoising methods have been developed under different frameworks, which can be broadly classified into two categories: frequency-domain and spatial-domain filtering [10]. Frequency-domain filtering works by generating a frequency-domain filter applied on a transformed image, such as Fourier transform and wavelet analysis [11], [12]. Although this type of filtering has been demonstrated to reduce the noise effectively, the requirement for spatial-to-frequency transformation during correction and vice versa can be considered a drawback of this approach, as it leads to longer overall processing time. In contrast, spatial-domain filtering methods typically perform correction by utilizing the statistical properties of pixel values in the input images, such as mean, standard deviation, or even histogram [13]–[15]. The benefit of this approach is that it can be performed without requiring spatial-to-frequency transformation, thus avoiding high computational costs. However, as this approach relies on the statistical properties of the images, for images with uneven pixel-value distribution, applying the global statistical properties to construct the filter might be irrelevant as it will lead to over-correction. Therefore, the availability of an adaptive spatial-based filter to avoid this problem is still required.

This work focuses on developing an algorithm that can reduce the stripe noise level on high-resolution satellite imageries, which manifests as vertical and horizontal line patterns in the images. As this type of noise can negatively impact the visual quality of the images, the goal of this work is to restore a clear satellite image from a given noisy image without introducing additional artifacts commonly emerging by existing methods [15], [16]. To achieve this goal, a combination of superpixel-based segmentation and statistics-

p-ISSN 2301–4156 | e-ISSN 2460–5719

based filtering is applied to each subregion. Superpixel segmentation groups similar pixels into larger and more significant areas, known as superpixels. Superpixels represent clusters of pixels with similar attributes like color, texture, or intensity, acting as the "building blocks" of an image. This method is essential for image segmentation as it simplifies image processing tasks and makes them more efficient by reducing the number of pixels [17].

In this work, a statistics-based noise removal introduced in [15] was applied for each subregion yielded by superpixel segmentation. The algorithm in [15] employed one-dimensional median and mean filters consecutively applied in vertical and horizontal directions. As this approach is originally applying an identical filter size on the entire image region, over-corrected artifacts commonly appeared on the resulting images, indicating that the filter size is not properly chosen. Therefore, to avoid a similar problem, in the proposed approach, the size of the median and mean filters was set to adaptively change, depending on the statistical properties of the subregions. In summary, the contribution of this work falls into two aspects. First, a novel stripe noise removal algorithm for satellite imageries based on superpixel segmentation and statistics-based filter is developed. This algorithm is then called superpixel-based stripe noise removal (SPSNR). The algorithm is capable of reducing the noise level without introducing additional artifacts. Second, the algorithm code and test datasets are publicly available so that other research communities with similar interests can use them in their case. The code can be downloaded from www.github.com/dancingpixel/SPSNR.

In order to assess the performance of the proposed algorithm, the algorithm has been tested on sixteen real imageries taken by LAPAN-A2 and LAPAN-A3 microsatellites. The evaluation was conducted by measuring the visual quality of the resulted images by using the peak-signal-to-noise ratio (PSNR) and structural similarity index (SSIM) metrics. Moreover, a benchmark test of the proposed algorithm to existing state-of-the-art stripe removal methods was performed.

Finally, the rest of this article is organized as follows: first, in Section II, the related works including the concept of superpixel-based segmentation and the existing statistics-based filtering is explained in detail. In Section III, the proposed algorithm is presented and the detail of the test dataset and assessment strategy are also elaborated. Finally, the experimental details and results is provided in Section IV, followed by the conclusion in Section V.

II. RELATED WORKS

In this section, the basic approaches employed in the proposed algorithm, i.e., superpixel-based segmentation and statistics-based filtering is presented in detail.

A. SUPERPIXEL-BASED SEGMENTATION

A superpixel can be defined as a collection of pixels that possesses homogeneous properties, including texture and color, and is frequently utilized in computer vision and image processing applications. The concept of superpixels involves consolidating pixels into more significant, easily processable regions that surpass the efficacy of analyzing individual pixels.

There are various methods available for superpixel segmentation, which can be grouped into three types: graph-based, gradient-based, and clustering-based algorithms.

Graph-based techniques take into consideration the image's brightness, contour, and texture, and generate superpixels that have a visually compact appearance [18], [19]. The normalized cut (NC) superpixel is an example that represents these methods [17]. Moreover, there is also an entropy rate superpixel (ERS), which relies on the entropy rate of random walk and an equilibrium term to generate superpixels with high segmentation accuracy [20]. Another widely adopted graph-based approach is the lazy random walk (LRW), which primarily takes into account the texture cues of the image [21].

In general, gradient-based superpixel segmentation can effectively adhere to object boundaries. Turbopixels is an example of a popularly adopted gradient-based superpixel that uses level-set technology to generate superpixels with linear computational complexity [22]. Another well-known technique is the watershed-based scheme which utilizes marker-controlled watershed transformation for superpixel segmentation [23]. In this instance, a spatially regularized gradient was applied to generate identical subregions.

The clustering-based approach generates superpixels through a linear iterative process offering a lower computational complexity especially compared to the graph-based approach [24]. The famous implementation of this approach was employing k-means simple linear iterative clustering (SLIC) [24]. SLIC is now considered as a state-of-the-art method for superpixel segmentation due to its ability to efficiently balance both spatial and color similarity while maintaining a short execution time. In addition, an intrinsic manifold SLIC capable of dealing with small-sized and high-intensity regions has also been introduced in [25]. Moreover, the edge-weighted centroidal Voronoi tessellations-based approach, known as VCell, is also among the popular clustering-based approaches that outperform traditional SLIC in addressing challenges such as boundary crossing and collision [26].

In this work, the SLIC was used as the backbone for the superpixel-based segmentation as it possesses both better segmentation accuracy and faster processing time compared to state-of-the-art algorithms [24]. The detailed implementation of the proposed approach is provided in Section III A.

B. STATISTICS-BASED STRIPE NOISE REMOVAL

The statistics-based method for removing stripe noise used for the proposed algorithm has been published [15]. The initial procedure for utilizing this algorithm involves extracting the vertical noise from the image by applying median filtering on the row direction followed by subtracting the median filtered image from the input image to form an initial noise template, T_{noise}. Afterward, vertically stretching the noise template using a mean filter will result in the final vertical noise template. The final noise template represents the extracted noise from the input image; hence, a recovered image can directly be resulted by subtracting this template from the original input image. As the steps explained are used to reduce the vertical stripe effect only, median filtering in column basis followed horizontal stretch on the resulting template.

In detail, removing vertical stripe noise using the method in can be done by following steps [15].

1. Assume there is an input image I and the pixel located at ith row index and jth column index is labeled as $I(i,j)$. To obtain the median filtered image $I_{MF}(i,j)$, perform a convolution operation in the horizontal direction between $I(i,j)$ and a global median filter template F_{MF}.

p-ISSN 2301–4156 | e-ISSN 2460–5719

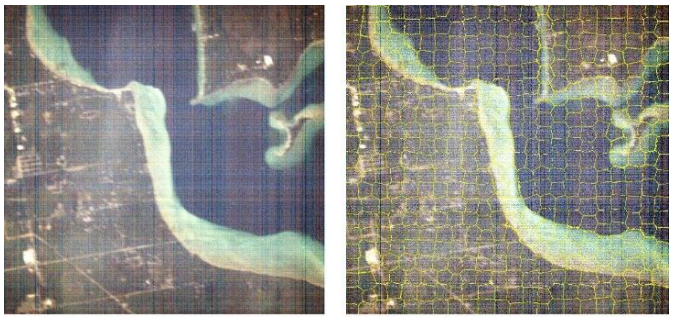

(a) (b)

Figure 1. Comparison of imageries with noise from superpixel segmentatin results, (a) imagery taken by LAPAN-A3 optical sensor containing stripe noises and (b) clustered regions based on superpixel segmentation using N = 500.

In this case, the F_{MF} is constructed by specifying a one-dimensional median filter size of N_{MF}.

$$I_{MF}(i,j) = I(i,j) \otimes F_{MF.} \quad (1)$$

2. To extract the initial noise template (T_{noise}), subtract the I_{MF} from the input image I.

$$T_{noise} = I - I_{MF.} \quad (2)$$

3. Stretch the T_{noise} template vertically by applying column-wise mean filter, F_{ME}. Similar to F_{MF}, a fixed-size N_{ME} must be set to the F_{ME} filter. The result of this step is called the final noise template, I_N.

$$I_N(i,j) = T_{noise}(i,j) \otimes F_{ME.} \quad (3)$$

4. Finally, recovered image I_C can be resulted by subtracting the I_N from the input image.

$$I_C = I - I_N. \quad (4)$$

It should be noted that all the steps above were designed specifically to reduce the presence of vertical stripe noise. To reduce the horizontal stripe noise, repeat the steps by first applying the F_{MF} in the vertical direction followed by stretching the T_{noise} horizontally.

III. METHODOLOGY

A. PROPOSED ALGORITHM

The proposed algorithm is dedicated to tackle common issues found while performing classical stripe noise, i.e., additional artifacts. In general, this artifact is produced as the effect of over-correction in a certain area of images caused by improper filter width selection while performing the filtering process. Therefore, a better way to determine filter size in suppressing the stripe noise based on superpixel segmentation is introduced in this work.

In this work, superpixel-based segmentation was employed to precisely cluster images into N subregions based on their texture and homogeneity so that regions with a high-intensity difference would be segmented partly. This strategy could ease the noise removal process as the filter size would be locally determined according to the statistical property of each cluster.

Figure 1(a) shows the example of a test image containing stripe noises spreading in both vertical and horizontal directions. It can be seen that the existence of this kind of noise degrades the visual quality of the image. In Figure 1(b), clustered regions are produced by superpixel-based segmentation. Figure 1(b) was converted into a grayscale colormap for better visualization. It is shown that the

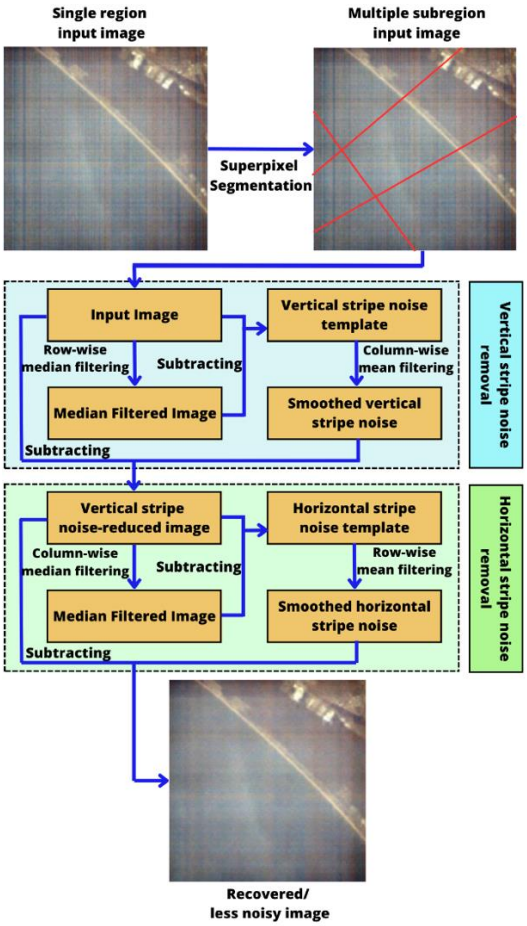

Figure 2. Flowchart of the proposed algorithm.

segmentation method is capable of clustering the images according to their intensity value in a precise manner.

The summary of the proposed algorithm which is the combination of superpixel-based segmentation and statistics-based stripe noise removal is given in Figure 2.

After applying the segmentation over an input image I, there would be N subregions that needed to be individually processed by using an adaptive statistics-based filter.

$$I = \{I_1, I_2, \ldots, I_N\}. \quad (5)$$

The term adaptive means that each of the median filter size (N_{MF}) or mean filter size (N_{ME}) will change dynamically according to the statistical properties of regions being corrected. In this work, the N_{MF} was set according to the standard deviation σ and maximum value of a subregion.

$$N_{MF}(k) = \left\lceil \left| \frac{\sigma(I_k)}{\max(I_k)} \right| \times N_{MF0} \right\rceil, k = 1, 2, \ldots, N. \quad (6)$$

According to (6), higher σ will lead to a wider filter size. The reason behind applying this strategy is that the σ value will be higher for a noisy subregion compared to the less noisy one, in turn, requires a larger N_{MF} size for extracting the initial noise template from the input image. The term N_{MF0} is a global constant representing a maximum median filter size. Similar to N_{MF}, the N_{ME} value was also set according to a statistical property as given below.

$$N_{ME}(k) = \left\lceil \frac{N_{nz}}{N_{pix}} \times N_{ME0} \right\rceil, k = 1, 2, \ldots, N. \quad (7)$$

The term N_{nz} and N_{pix}, respectively, represent the number of nonzero pixels and the total pixel population of the initial noise

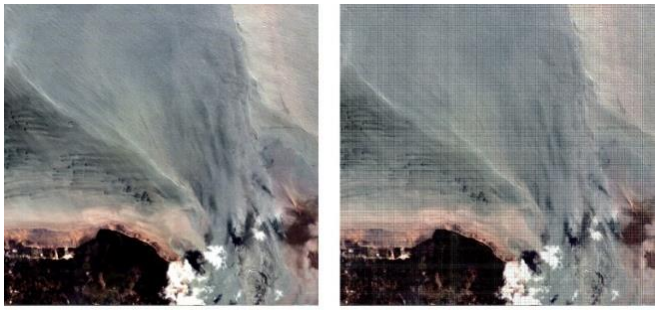

(a) (b)

Figure 3. Examples of synthetically-generated stripe noisy image, (a) an input image from LAPAN-A2 dataset, (b) noisy version after being added by synthetic stripe.

TABLE I
PARAMETERS USED FOR THE EXPERIMENT

Dataset	Image Count	Dimension	Average PSNR (dB)
LAPAN-A2	6	2048 × 2048 × 3	17.162
LAPAN-A3	10	2044 × 2047 × 3	15.619

template (T_{noise}) previously extracted by the median filter chain. Since the mean filter was applied to T_{noise}, the N_{nz} was the number of pixels considered as noise, and therefore the higher the N_{nz}, the wider the N_{ME}. Then, the term N_{ME0} is also introduced, which is assigned as the maximum possible filter size.

B. EVALUATION STRATEGY

In order to evaluate the performance of the proposed method, the quality of the recovered image and the processing time required by the method was measured. Both of these variables are essential to assess whether the algorithm is well-performing.

To measure image quality, the PSNR and SSIM metrics were employed. The PSNR represents the ratio of the highest signal to noise background and the higher the PSNR indicates the lower the noise. The other metric, SSIM, was used to measure the similarity level between two images. Mathematical representation of PSNR and SSIM metric is given in (8) and (9).

$$PSNR = 20log_{10}\left(\frac{max(I_i)}{\sqrt{MSE}}\right) \quad (8)$$

$$SSIM\ (x,y) = \frac{(2\eta_x\eta_y)(2\sigma_{xy})}{(\eta_x^2+\eta_y^2)(\sigma_x^2+\sigma_y^2)}. \quad (9)$$

Equation (9) was used to calculate SSIM values between image x and y; meanwhile, the η_x, η_y, σ_x, σ_x, and σ_{xy} refer to the average value of x, the average value of y, variance of x, variance of y, and covariance of x and y. Besides representing the similarity level between the recovered and reference images, the SSIM metric can also be used as an indicator of the existence of additional artifacts as the artifacts would introduce a new structure to the image and consequently lower the SSIM value.

As the SSIM measurement requires a reference image, instead of using a noisy LAPAN-A3 dataset in this work, images on a less-noisy dataset produced by the LAPAN-A2 satellite were used as the references. The synthetic noisy images were created by adding stretched random noise to form the stripe pattern. In the end, the synthetic images were then passed to the proposed algorithm, and the SSIM between the recovered and reference images was measured. An example of a synthetically-generated stripe noisy image is shown in Figure 3.

TABLE II
PARAMETERS USED FOR THE EXPERIMENT

Parameter	Symbol	Value
Subregion count	N	500
Maximum median filter width	N_{MF0}	300
Maximum mean filter width	N_{ME0}	300

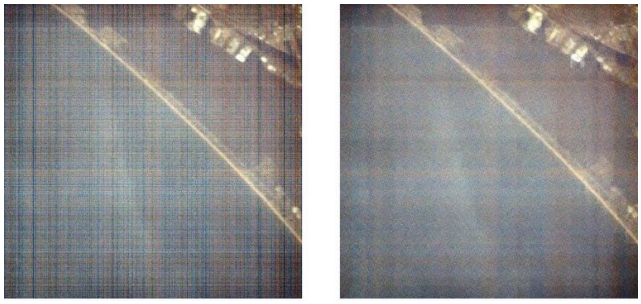

(a) (b)

Figure 4. Visual comparison of input images and their recovered versions, (a) an input image from LAPAN-A3 dataset, (b) the recovered image using the proposed method.

C. DATASET USED

There are two optical imagery datasets used in this work, i.e., LAPAN-A2 and LAPAN-A3. Each image on both datasets was taken at a different location and day. Both datasets were captured by identical onboard sensors of LAPAN-A2 and LAPAN-A3 satellites with a resolution of 4.5 m. The images on LAPAN-A2 dataset are less noisy (higher PSNR) compared to the latter. Therefore, this dataset was used as ideal reference images when measuring SSIM. The other dataset, LAPAN-A3, had a higher noise level in terms of PSNR value and was used for evaluating the capability of the proposed method in reducing noise. Table I shows the properties of both datasets.

IV. RESULT AND DISCUSSION

In this section, the evaluation results of the proposed method including the quality of resulted images are presented. Moreover, the performance comparison of the proposed method to the state-of-the-art algorithms in terms of image quality and processing speed is also provided.

A. QUALITATIVE IMAGE ASSESSMENT

The first experiment was conducted by passing LAPAN-A3 dataset to the proposed algorithm in order to assess the capability of the algorithm in dealing with noisy images. The parameters used in the experiments were empirically determined and are given in Table II. Since each channel of the test image consists of around 4 million pixels, in this work, dividing the image into 500 subregions containing 8,000-10,000 pixels was sufficient to encapsulate relatively small objects, such as cloud blobs and man-made features. Moreover, both global filters' size N_{MF0} and N_{ME0} to 300 has also been assigned as it minimizes blurry effect on the resulted images.

From Figure 4, it can be seen that the proposed algorithm is capable of reducing the noise disturbance on the recovered image. The stripe effect that is commonly found on the input image (Figure 4(a)) is depleted in the recovered image (Figure 4(b)). This result can be used to verify that the proposed algorithm is well-performing according to visual inspection.

Since the filter size of the proposed method, NMF and NME, is adaptively changing, it is found that the resulting images are insensitive to additional artifacts, which are commonly found in fixed-size filter implementation. As shown in Figure 5, the

p-ISSN 2301–4156 | e-ISSN 2460–5719

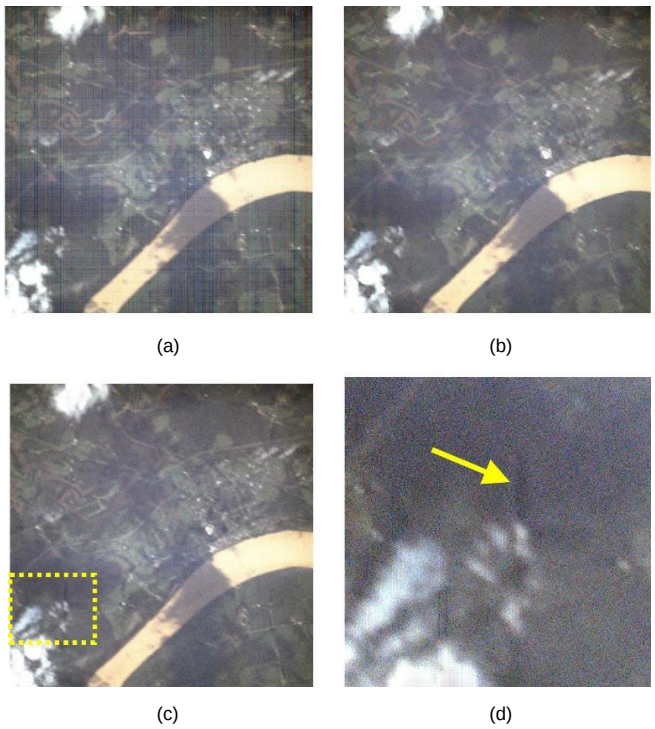

Figure 5. Visual comparison of input images and their recovered versions with adaptively-changing filter size (a) an input image, (b) the recovered image with adaptively-changing filter size, (c) image recovered using fixed-size filter, (d) zoomed yellow-boxed area.

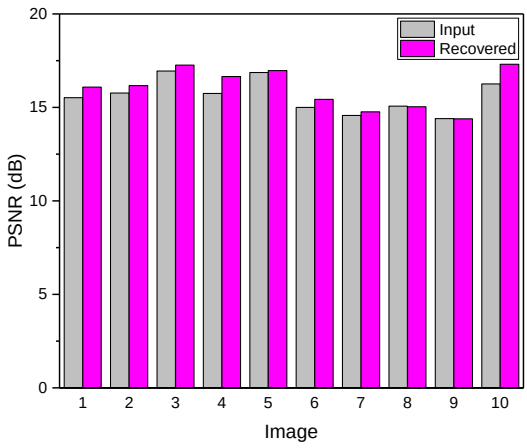

Figure 6. Comparison of PSNR value between input noisy images and recovered images through the proposed method using LAPAN-A3 dataset.

proposed algorithm provides better results regarding the absence of artifacts compared to the existing method presented in [15]. Figure 5(a) shows an input image from LAPAN-A3 dataset; meanwhile, Figure 5(b) is the recovered image using adaptively-changing filter sizes of the proposed method. Figure 5(c) presents an image recovered using fixed-size filter with NMF = 300 and NME = 300, while Figure 5(d) is the zoomed yellow-boxed area of image in Figure 5(c), showing additional artifacts as pointed by the yellow arrow.

B. QUANTITATIVE IMAGE QUALITY ASSESSMENT

In order to quantitatively measure the performance of the proposed algorithm in terms of reducing the noise level, the PSNR on both the input and recovered images of LAPAN-A3 datasets was calculated, and the result was then compared.

According to Figure 6, it can be seen that applying the proposed algorithm increase the PSNR value on almost all recovered images indicating that the method has been working properly in the noise reduction case.

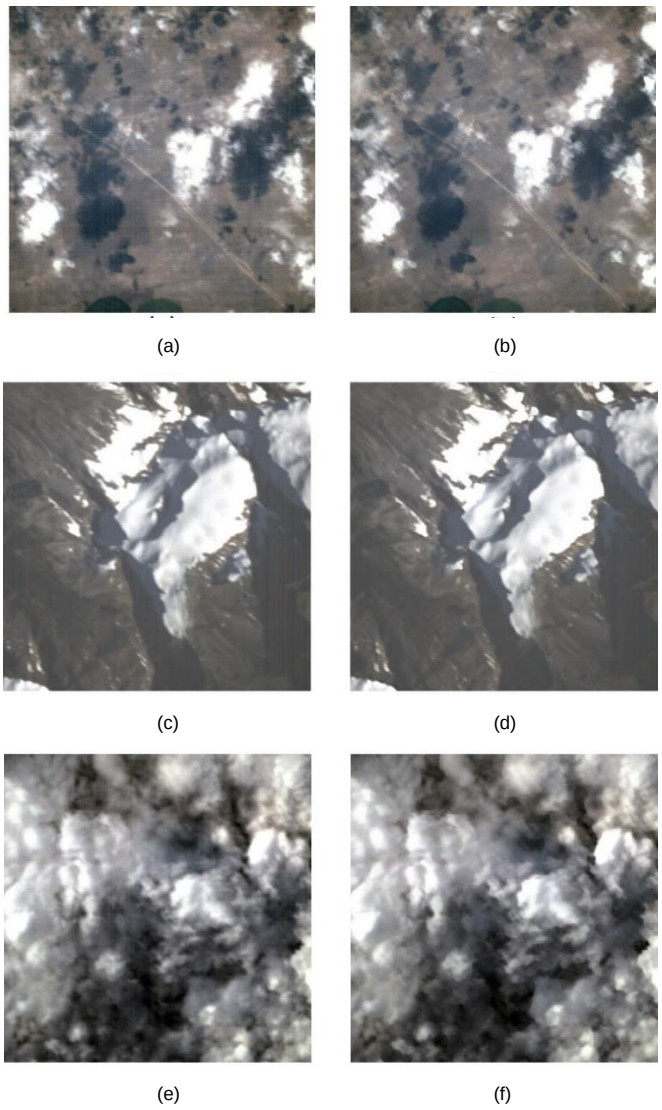

Figure 7. Comparison of noisy images and their recovered version from th implementation of the proposed algorithm, (a) noisy image of “Image 5”, (b) recovered image of “Image 5”, (c) noisy image of “Image 8”, (d) recovered image of “Image 8”, (e) noisy image of “Image 9”, and (f) recovered image of “Image 9”.

The biggest PSNR increment was found in the case of recovered “Image 10” with a 6.46% increase, while the PSNR of recovered “Image 5”, “Image 8”, and “Image 9” were closely similar to those of their noisy input. One might think that the proposed method is ineffective for those images; however, by viewing Figure 7, it is clear that the stripe pattern effect appears to be diminishing, improving the visual quality of the recovered version of those images.

The most possible reason for this particular case is that evaluating the visual quality using the PSNR metric is sometimes insufficient, and therefore the SSIM metrics were employed for the assessment in the next section. Finally, based on the calculation, the average PSNR value of this dataset was improved by 2.46% after the correction, verifying that the proposed algorithm improves the visual quality and lowers the disturbing noise.

C. PERFORMANCE COMPARISON

In this section, result of the performance benchmark in terms of SSIM and computing speed of the proposed algorithm to three existing methods is reported. The first method was a pure statistics-based stripe noise removal employing fixed-size filters as introduced in [15], which was also the base of the

p-ISSN 2301–4156 | e-ISSN 2460–5719

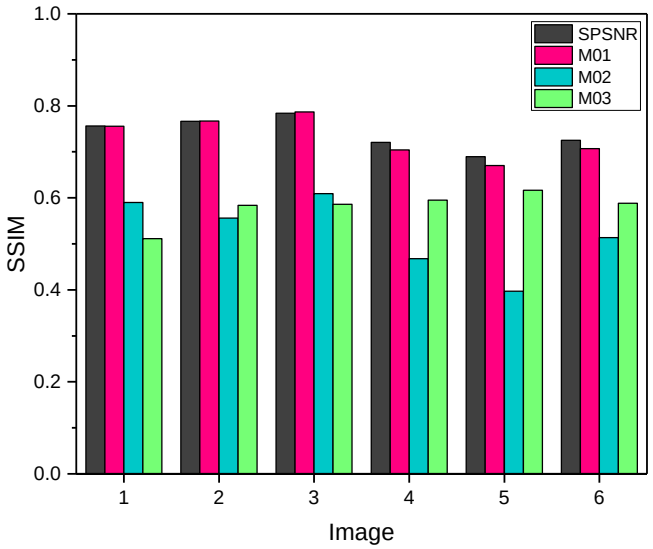

Figure 8. Comparison of SSIM value between input and recovered images using different methods.

TABLE III
COMPARISON OF COMPUTATION SPEED

Image	Computation Speed (s)			
	SPSNR	***M01***	***M02***	***M03***
1	6.969	1.301	272.660	640.158
2	6.075	1.311	275.714	636.838
3	6.001	1.310	269.016	623.430
4	6.017	1.307	261.363	662.966
5	7.155	1.300	261.697	695.480
6	6.018	1.312	260.583	707.909
Average	6.372	1.307	266.839	661.130

proposed method. The second method was the improved version of the first method with the involvement of weighting schema in determining the size of filters. The detailed implementation of the second method can be found in [16]. The last method was introduced in [27], which used sheared decomposition framework for oblique stripe removal. This method has been tested and is well-performing in the case of Terra MODIS and Landsat 7 imageries. For the sake of simplicity, all the existing methods were then called as "M01", "M02" and "M03", while the proposed algorithm used the "SPSNR" term.

According to Figure 8, the proposed SPSNR algorithm is generally better than the other methods in terms of recovering an accurate image. It is shown that the accuracy provided by SPSNR which is stated in SSIM value is ranging from 0.67 to 0.78. In contrast, its competitors only produced SSIM between 0.39 to 0.77. By averaging over all the images, the highest average accuracy of 0.74 was reserved by SPSNR followed by M01, M03, and M02 with accuracies of 0.73, 0.58, and 0.52, respectively.

In this work, the speed benchmarking was run on Windows 11 machine, equipped with Intel® Xeon W-2223 8 CPUs @3.60 GHz processor and 64 GB of RAM. By looking at Table III, it is clear that the traditional statistics-based method (M01) is superior compared to others with an average speed of only 1.3 seconds. This condition is reasonable since the M01 method did not perform any preprocessing steps like SPSNR, M02, and M03 did. The slow speed by SPSNR was mainly caused by the superpixel segmentation stage while the slow performance by the M02 was found on pixel-wise weighting for determining filter size. The most surprising result is that the M03 was almost 103 times slower than the proposed method as it performed massive group sparsity calculations requiring high computational load. Last but not least, by comparing the M02 and SPSNR, it was found that SPSNR was superior with a speed gain of 41.87.

Finally, based on the SSIM comparison in Figure 8, it can also be inferred that the M02 and M03 perform poorly in the case of LAPAN-A2 dataset. There are two possibilities causing low SSIM values of recovered images produced by those methods. First, the characteristics of the input images used in the proposed experiments may not be suitable enough to make the methods work properly. Second, the use of improper parameters could be another reason as this work directly used the value provided in the reference paper. Therefore, a fine-tuning schema might be required for further use of the methods.

V. CONCLUSION

In this work, a novel stripe noise removal algorithm based on the combination of superpixel segmentation and statistics-based filtering has been introduced. The algorithm was tested using real satellite imageries taken by LAPAN-A2 and LAPAN-A3 satellites and its performance was compared to three existing methods in terms of image quality and computation speed. Based on the experiment, the proposed algorithm was proven capable of improving the image quality by 2.46% and had around 42–103 times faster execution speed compared to its competitors. Finally, the proposed algorithm, in concept, can be employed to reduce the stripe noise effect on various types of images, however, finely tuning the associated parameters is highly recommended.

CONFLICT OF INTEREST

The authors declare no conflict of interest.

AUTHOR CONTRIBUTION

Conceptualization, Kamirul and Khairunnisa; methodology, Kamirul, Khairunnisa, and Agus Herawan; software, Kamirul, and Dicka Ariptian Rahayu; validation, Ega Asti Anggari, Moedji Soedjarwo, and Chusnul Tri Judianto; formal analysis, Kamirul; investigation, Khairunnisa; resources, Dicka Ariptian Rahayu; data curation, Kamirul and Dicka Ariptian Rahayu; writing—original draft preparation, Kamirul; writing—review and editing, Khairunnisa; visualization, Khairunnisa; supervision, Chusnul Tri Judianto; project administration, Kamirul.

ACKNOWLEDGMENT

The authors would like to thank the Research Center for Satellite Technology – National Research and Innovation Agency (Badan Riset dan Inovasi Nasional, BRIN) for providing the LAPAN-A2 and LAPAN-A3 datasets.

REFERENCES

[1] D. Wang *et al.*, "SSRNet: In-Field Counting Wheat Ears Using Multi-Stage Convolutional Neural Network," *IEEE Trans. Geosci., Remote Sens.*, Vol. 60, pp. 1–11, 2022, doi: 10.1109/TGRS.2021.3093041.

[2] X. Zhang *et al.*, "Convective Clouds Extraction From Himawari–8 Satellite Images Based on Double-Stream Fully Convolutional Networks," *IEEE Geosc., Remote Sens. Lett.*, Vol. 17, No. 4, pp. 553–557, Apr. 2020, doi: 10.1109/LGRS.2019.2926402.

[3] S. Lee and D. Shin, "On-Orbit Camera Misalignment Estimation Framework and Its Application to Earth Observation Satellite," *Remote Sens.*, Vol. 7, No. 3, pp. 3320–3346, Mar. 2015, doi:10.3390/rs70303320.

[4] F.J. Meyer, J.B. Nicoll, and A.P. Doulgeris, "Correction and Characterization of Radio Frequency Interference Signatures in L-Band

p-ISSN 2301–4156 | e-ISSN 2460–5719

Synthetic Aperture Radar Data," *IEEE Trans. Geosci. Remote Sens.*, Vol. 51, No. 10, pp. 4961–4972, Oct. 2013, doi: 10.1109/TGRS.2013.2252469.

[5] L. Zhuang and M.K. Ng, "Cross-Track Illumination Correction for Hyperspectral Pushbroom Sensors Using Total Variation and Sparsity Regularization," *2020 IEEE 11th Sensor Array, Multichannel Signal Process. Workshop (SAM)*, 2020, pp. 1–5, doi: 10.1109/SAM48682.2020.9104285.

[6] M. Amrouche, H. Carfantan, J. Idier, and V. Martin, "Statistical Destriping of Pushbroom-Type Images Based on an Affine Detector Response," *IEEE Trans. Geosci., Remote Sens.*, Vol. 60, pp. 1–14, Jul. 2022, doi: 10.1109/TGRS.2022.3195092.

[7] B. Zhang *et al.*, "Hyperspectral Image Stripe Detection and Correction Using Gabor Filters and Subspace Representation," *IEEE Geosci. Remote Sens. Lett.*, Vol. 19, pp. 1–5, 2022, doi: 10.1109/LGRS.2021.3061541.

[8] Q. Wang, X. Ding, X. Tong, and P. M. Atkinson, "Real-Time Spatiotemporal Spectral Unmixing of MODIS Images," ," *IEEE Trans. Geosci., Remote Sens.*, Vol. 60, pp. 1–16, 2022, doi: 10.1109/TGRS.2021.3108540.

[9] W. Teng *et al.*, "Classifier-Constrained Deep Adversarial Domain Adaptation for Cross-Domain Semisupervised Classification in Remote Sensing Images," *IEEE Geosci. Remote Sens. Lett.*, Vol. 17, No. 5, pp. 789–793, May 2020, doi: 10.1109/LGRS.2019.2931305.

[10] Y. Chang, L. Yan, T. Wu, and S. Zhong, "Remote Sensing Image Stripe Noise Removal: From Image Decomposition Perspective," *IEEE Geosci. Remote Sens. Lett.*, Vol. 54, No. 12, pp. 7018–7031, Dec. 2016, doi: 10.1109/TGRS.2016.2594080.

[11] Q. Zeng, H. Qin, X. Yan, and H. Zhou, "Fourier Spectrum Guidance for Stripe Noise Removal in Thermal Infrared Imagery," *IEEE Geosci. Remote Sens. Lett.*, Vol. 17, No. 6, pp. 1072–1076, Jun. 2020, doi: 10.1109/LGRS.2019.2938822.

[12] M. Li *et al.*, "A Novel Stripe Noise Removal Model for Infrared Images," *Sensors*, Vol. 22, No. 8, pp.1–22, Apr. 2022, doi: 10.3390/s22082971.

[13] J. Lin, H. Zuo, Y. Ye, and X. Liao, "Histogram-Based Autoadaptive Filter for Destriping NDVI Imagery Acquired by UAV-Loaded Multispectral Camera," *IEEE Geosci. Remote Sens. Lett.*, Vol. 16, No. 4, pp. 648–652, Apr. 2019, doi: 10.1109/LGRS.2018.2877728.

[14] S. Banerjee and P. Shanmugam, "An Improved Method for Destriping of VIIRS Day/Night Band Images," *IEEE Access*, Vol. 10, pp. 82164–82184, Jul. 2022, doi: 10.1109/ACCESS.2022.3194053.

[15] Kamirul, P.R. Hakim, and S. Salaswati, "Statistical-based Stripe Noise Correction on LAPAN Microsatellite Imagery," *2018 IEEE Int. Conf. Aerosp. Electron. Remote Sens. Technol. (ICARES)*, 2018, pp. 72–77, doi: 10.1109/ICARES.2018.8547079.

[16] Kamirul, P.R. Hakim, and W. Hasbi, "An Adaptive Stripe Noise Removal Algorithm for Optical Satellite Imagery," *2019 IEEE Int. Conf. Aerosp. Electron., Remote Sens. Technol. (ICARES)*, 2019, pp. 1–7, doi: 10.1109/ICARES.2019.8914344.

[17] S. Subudhi, R.N. Patro, P.K. Biswal, and F. Dell'Acqua, "A Survey on Superpixel Segmentation as a Preprocessing Step in Hyperspectral Image Analysis," *IEEE J. Sel. Topics Appl. Earth Observ., Remote Sens.*, Vol. 14, pp. 5015–5035, Apr. 2021, doi: 10.1109/JSTARS.2021.3076005.

[18] L. Yang *et al.*, "Semisupervised Hyperspectral Image Classification via Superpixel-Based Graph Regularization with Local and Nonlocal Features," *IEEE J. Sel. Topics Appl. Earth Observ., Remote Sens.*, Vol. 15, pp. 6645–6658, Jul. 2022, doi: 10.1109/JSTARS.2022.3191692.

[19] T. Ince, "Superpixel-Based Graph Laplacian Regularization for Sparse Hyperspectral Unmixing," *IEEE Geosci. Remote Sens. Lett.*, Vol. 19, pp. 1–5, 2022, doi: 10.1109/LGRS.2020.3027055.

[20] M.-Y. Liu, O. Tuzel, S. Ramalingam and R. Chellappa, "Entropy-Rate Clustering: Cluster Analysis via Maximizing a Submodular Function Subject to a Matroid Constraint," *IEEE Trans. Pattern Anal., Mach. Intell.*, Vol. 36, No. 1, pp. 99–112, Jan. 2014, doi: 10.1109/TPAMI.2013.107.

[21] J. Shen, Y. Du, W. Wang, and X. Li, "Lazy Random Walks for Superpixel Segmentation," *IEEE Trans. Image Process.*, Vol. 23, No. 4, pp. 1451–1462, Apr. 2014, doi: 10.1109/TIP.2014.2302892.

[22] A. Levinshtein *et al.*, "TurboPixels: Fast Superpixels Using Geometric Flows," *IEEE Trans. Pattern Anal., Mach. Intell.*, Vol. 31, No. 12, pp. 2290–2297, Dec. 2009, doi: 10.1109/TPAMI.2009.96.

[23] Y. Yuan, Z. Zhu, H. Yu and W. Zhang, "Watershed-Based Superpixels with Global and Local Boundary Marching," *IEEE Trans. Image Process.*, Vol. 29, pp. 7375–7388, Jun. 2020, doi: 10.1109/TIP.2020.3002078.

[24] R. Achanta *et al.*, "SLIC Superpixels Compared to State-of-the-Art Superpixel Methods," *IEEE Trans. Pattern Anal., Mach. Intell.*, Vol. 34, No. 11, pp. 2274–2282, Nov. 2012, doi: 10.1109/TPAMI.2012.120.

[25] Y.-J. Liu, M. Yu, B.-J. Li and Y. He, "Intrinsic Manifold SLIC: A Simple and Efficient Method for Computing Content-Sensitive Superpixels," *IEEE Trans. Pattern Anal., Mach. Intell.*, Vol. 40, No. 3, pp. 653–666, Mar. 2018, doi: 10.1109/TPAMI.2017.2686857.

[26] Y. Zhou, L. Ju, and S. Wang, "Multiscale Superpixels and Supervoxels Based on Hierarchical Edge-Weighted Centroidal Voronoi Tessellation," *2015 IEEE Winter Conf. Appl. Comput. Vis.*, 2015, pp. 1076–1083, doi: 10.1109/WACV.2015.148.

[27] J. Wang *et al.*, "A Sheared Low-Rank Model for Oblique Stripe Removal," *Appl. Math. Comput.*, Vol. 360, pp. 167–180, Nov. 2019, doi: 10.1016/j.amc.2019.03.066.